Downloaded from orbit.dtu.dk on: Apr 29, 2024

DTU Library

Three-Dimensional in Situ Electron-Beam Lithography Using Water Ice

Hong, Yu; Zhao, Ding; Liu, Dongli; Ma, Binze; Yao, Guangnan; Li, Qiang; Han, Anpan; Qiu, Min

Published in:
Nano Letters

Link to article, DOI:
10.1021/acs.nanolett.8b01857

Publication date:
2018

Document Version
Peer reviewed version

Link back to DTU Orbit

Citation (APA):
Hong, Y., Zhao, D., Liu, D., Ma, B., Yao, G., Li, Q., Han, A., & Qiu, M. (2018). Three-Dimensional in Situ Electron-Beam Lithography Using Water Ice. *Nano Letters*, *18*(8), 5036–5041. https://doi.org/10.1021/acs.nanolett.8b01857

General rights
Copyright and moral rights for the publications made accessible in the public portal are retained by the authors and/or other copyright owners and it is a condition of accessing publications that users recognise and abide by the legal requirements associated with these rights.

- Users may download and print one copy of any publication from the public portal for the purpose of private study or research.
- You may not further distribute the material or use it for any profit-making activity or commercial gain
- You may freely distribute the URL identifying the publication in the public portal

If you believe that this document breaches copyright please contact us providing details, and we will remove access to the work immediately and investigate your claim.

Three-dimensional *in situ* Electron Beam Lithography Using Water Ice

Yu Hong[1,‡], Ding Zhao[1,‡,], Dongli Liu[2,3], Binze Ma[1], Guangnan Yao[1], Qiang Li[1], Anpan Han[4] and Min Qiu[1,2,3,*]*

[1]State Key Laboratory of Modern Optical Instrumentation, College of Optical Science and Engineering, Zhejiang University, Hangzhou 310027, P.R. China.

[2]Institute for Advanced Technology, Westlake Institute for Advanced Study, Hangzhou 310024, P.R. China.

[3]Westlake University, Hangzhou 310030, P.R. China.

[4]DTU Danchip/Cen, Technical University of Denmark, Kongens Lyngby 2800, Denmark

KEYWORDS: nanofabrication, three-dimensional nanostructures, electron beam lithography, ice resists, ice lithography

ABSTRACT: Three-dimensional (3D) nanofabrication techniques are of paramount importance in nanoscience and nanotechnology as they are prerequisites to realize complex, compact, and functional 3D nanodevices. Though several 3D nanofabrication methods have been proposed and developed in recent years, it is still a formidable challenge to achieve a balance among resolution, accuracy, simplicity, and adaptability. Here we propose a 3D nanofabrication method based on electron beam lithography using ice resists (iEBL) and fabricate 3D nanostructures by stacking

layered structures and dose-modulated exposing, respectively. The whole process of 3D nanofabrication is realized in one vacuum system by skipping spin-coating and developing steps required for commonly used resists. This needs much less processing steps and is contamination-free as compared to conventional methods. With *in situ* alignment and correction in the iEBL process, a pattern resolution of 20 nm and an alignment error below 100 nm can be steadily achieved. This 3D nanofabrication technique using ice thus shows great potential in fabrication of complicated 3D nanodevices.

Three-dimensional (3D) nanofabrication towards tailoring functional materials with desired nanostructures is extremely important in nanoscience, nanotechnology and interdisciplinary fields, such as nanophotonics[1-3], electronics[4,5], bionics[6,7], biomedical engineering[8,9] and energy engineering[10-12]. Though several 3D nanofabrication methods have been proposed and developed in recent years, it is still a great challenge to achieve a balance among resolution, accuracy, simplicity, and adaptability. For example, three-dimensional printing (3DP), such as inkjet printing[13], direct writing[14], and dynamic-optical-projection stereolithography[15], have advantages in custom manufacturing, but the resolution of these methods is usually over 1 μm[16]. High-resolution 3DP methods, such as electro-hydrodynamic inkjet printing (e-jetP)[17] and two-photon polymerization (TPP)[18,19], can achieve the spatial resolution down to 50 nm[20] and 40 nm[21,22], respectively. Nevertheless, e-jetP is unstable during ejection and stacking process, while the material for TPP is required to be transparent and photopolymerizable[23], which undoubtedly imposes crucial limitation in its applications.

Unlike 3DP methods, electron beam lithography (EBL), focused electron-beam-induced deposition (FEBID)[24], and scanning probe lithography (SPL)[25] have both high resolution and material flexibility. However, 3D nanofabrication by stacking layered structures using EBL, where each layer obtained through repeating a standard spin-coating – lithography – developing – deposition (or etching) – lift-off processes, takes relatively longer overall fabrication time, especially for complex 3D nanostructures. The overlay alignment is typically realized through alignment masks, and the overall procedures are tedious, expensive and difficult to master. Although the direct-write nature of FEBID enables high flexibility in the design of 3D nanostructures, the dissociation of precursors usually leaves unwanted carbon fraction in the deposit resulting in serious carbon contamination. Moreover, both FEBID and SPL are more time-consuming than EBL and expensive to carry out in some cases.

Constructing 3D functional polymer brushes is another promising strategy to realize 3D nanostructures, where polymer brushes are usually obtained through nanofabrication of surface initiators and subsequent polymerization. It has been shown that surface initiators can be patterned by EBL[26] and SPL[27]. For instance, dip-pen nanodisplacement lithography (DNL) is a versatile scanning-probe-based approach for manipulating polymer brushes at the nanometer scale[28], which has very high resolution and registration. Other modified lithography methods developed for 3D nanofabrication, such as nanoimprint[29] and nanotransfer printing[30], rely on a pre-generated template or stamp. Self-assembly methods, such as colloidal lithography[31] and block copolymer lithography[32], are simple and cost-effective, but the shape and size of products are restricted by the additives.

Electron beam lithography utilizing ice resists (iEBL), also called ice lithography, has emerged for nanofabrication with high resolution[33], even on nonplanar and fragile substrates[34,35]. It has been shown that water ice acts as a positive resist while organic ice, such as anisole ice, is usually a negative resist[36,37]. In iEBL, the standard process is greatly simplified and streamlined by skipping spin-coating and developing steps[38]. Notably, ice resists covering substrates maintain the shape of substrates or previously fabricated nanostructures, which can be clearly distinguished by SEM imaging. Attributing to the very low sensitivity of water ice, iEBL enables *in situ* alignment and correction with the previous layer. This feature is significantly beneficial to the improvement of overlay alignment accuracy. Moreover, ice is easily removed without leaving any residue by simply raising the temperature during the lift-off step, providing great potential to fabricate suspended or hollow structures. These advantages make iEBL an excellent candidate for 3D nanofabrication.

Here, we demonstrate experimentally two strategies for 3D nanofabrication using water ice. One is stacking layered structures, and the other one is dose-modulated exposing. All experiments are performed in a dedicated vacuum system (See Figure S1 in Supporting Information for details) consisting of a modified scanning electron microscope (SEM) and a metal deposition chamber. An outline of the typical iEBL process is presented in Figure 1. The sample is cooled by a sample holder at 130 K (Figure 1a), then saturated water vapor is injected onto the sample to form an amorphous ice layer (Figure 1b). The ice thickness is controlled by adjusting the amount of injected water vapor. The ice is removed during e-beam exposure (Figure 1c), and a pattern with almost vertical side wall can be achieved, which makes it possible to *in situ* measure the thickness of water ice by tilting the sample in SEM (See Figure S2 in Supporting Information for details). After

metallization (Figure 1d), the sample is taken out from the system and immediately immersed into alcohol for lift-off (Figure 1e). It is known that solid water will experience a volume change when a phase change occurs. This is detrimental to iEBL since the volume change of ice mask may reshape the fabricated 3D nanostructures. Considering the whole process of iEBL, phase change probably occurs only when lift-off, due to the increase of sample temperature and ambient pressure. However, we have not noted any significant effect on fabricated samples induced by this issue (See Figure S3 in Supporting Information for details).

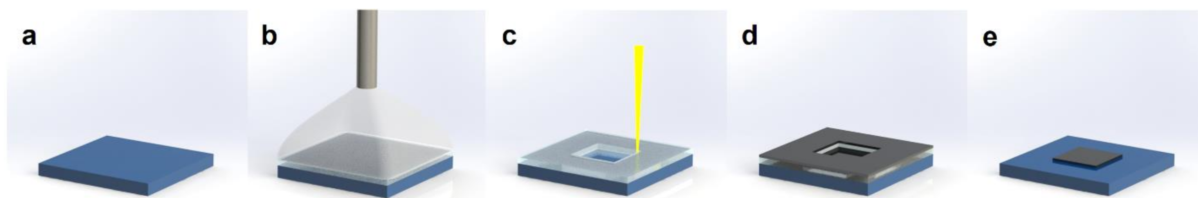

Figure 1. Process of EBL using water ice resists. (a) Refrigeration: the stage is cooled to 130 K. (b) Deposition: water vapor is deposited onto the sample to form ice resist. (c) Exposure: the ice resist exposed by e-beam is eliminated. (d) Metallization: the metal film is deposited onto the sample. (e) Lift-off: the sample is immersed into alcohol to remove ice resists.

3D nanostructures can be easily fabricated by iEBL through stacking layered structures. The process flow of a stepped pyramid is shown in Figure 2. The iEBL processes, including ice forming, e-beam patterning, and metal deposition, are repeated three times. At each time, the thicknesses of ice resist and Ag deposit are maintained 300 nm and 60 nm, respectively. *In situ* SEM images of the first ice layer on a silicon substrate before and after 20 keV e-beam patterning are shown in Figures 2a and 2b, respectively. Ag film is subsequently deposited (Figure 2c), and a Ag stepped pyramid surrounded by ice/Ag multilayers is achieved by repeating above mentioned processes illustrated in Figures 2d-2i. Due to the limited temperature of our cooling system, the

ice layer sublimated slightly and recrystallized on the sample during processing, resulting in uneven surfaces of the substrate and subsequent metal structures. This problem may be resolved using a sample stage with lower temperature[33]. Figures 2j-2l show SEM images and an atomic force microscope (AFM) line scan of the 3D nanostructure after lift-off. As mentioned before, it is an extremely tedious process for fabricating such 3D pyramidal nanostructure by standard EBL, where at least 19 processing steps and 8 load-unload operations (in and out of the vacuum system) of the sample are required. While for iEBL, only 10 processing steps are needed here (see the comparative Figure S4 in Supporting Information), and all in the same vacuum system except the final lift-off step. Overall, only single load-unload operation and one-off lift-off step are performed during iEBL, regardless of how many layers are fabricated. This technique effectively reduces possible contamination to the sample and time consumption caused by repetitive pumping and venting of the vacuum chamber.

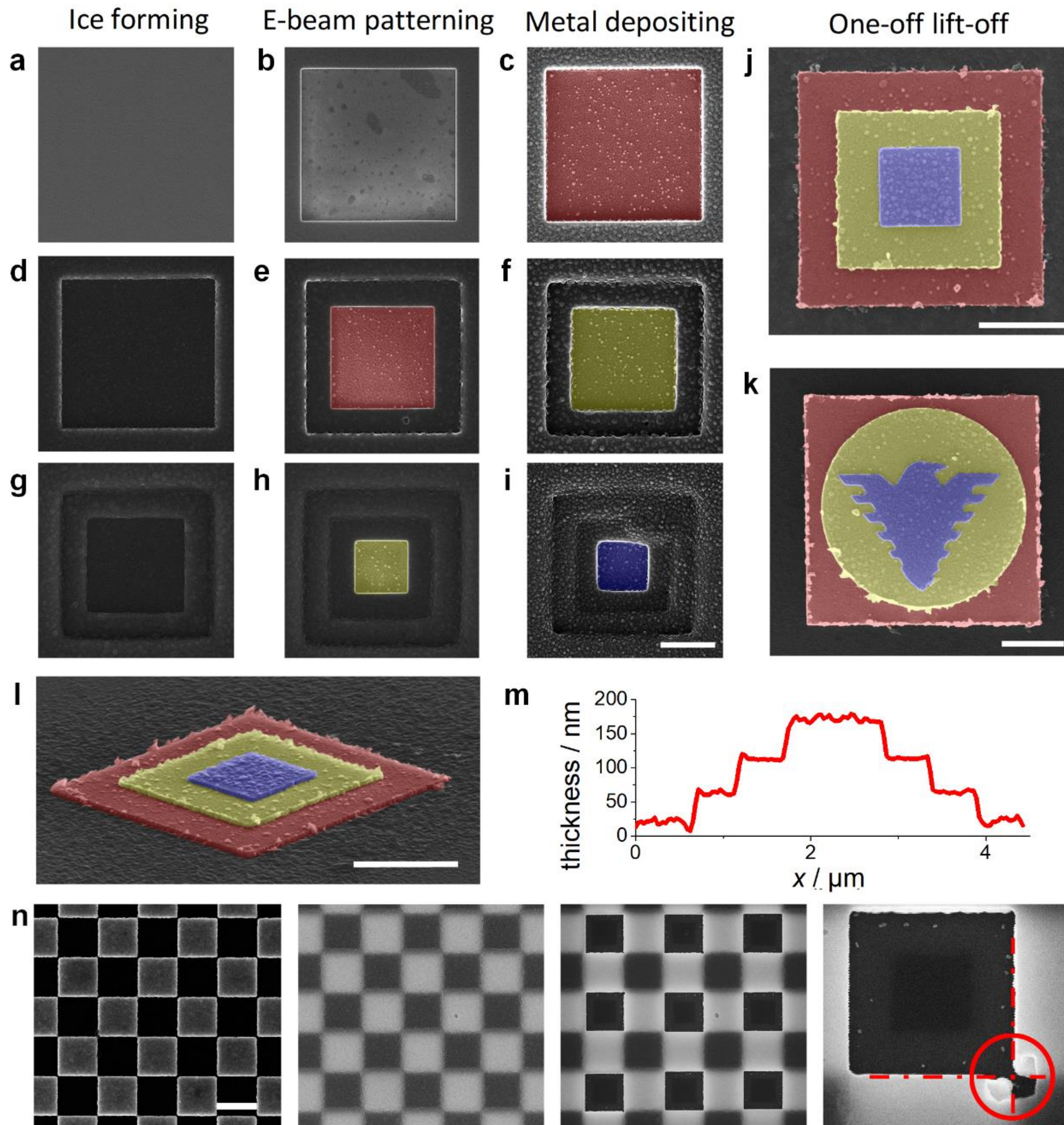

Figure 2. 3D pyramidal nanostructure fabricated by iEBL and *in situ* cryogenic SEM imaging. (a), (d) and (g) *In situ* cryogenic SEM images of 300-nm-thick ice resists at different stages deposited onto the sample. (b), (e) and (h) *In situ* cryogenic SEM images of 3 μm × 3 μm, 2 μm × 2 μm and 1 μm × 1 μm squares formed in the ice resists by a 20 keV, 150 pA electron beam. The e-beam patterning dose is 0.8 C/cm^2. (c), (f) and (i) *In situ* cryogenic SEM images of 60-nm-thick Ag films deposited onto the sample. (j) and (l) Room-temperature SEM images of the fabricated 3D pyramidal nanostructure after final lift-off. Squares indicate full and partial areas of each Ag layer

in the 3D pyramidal nanostructure. (k) SEM image of the fabricated 3D multilayered nanostructure with the shape of eagle logo. Note that the SEM images in (c), (e), (f), (h), (j), (k) and (l) are false colored for enhancing visual illustration. (m) Central line scan of the 3D pyramidal nanostructure (l) by atom force microscope (AFM). The root-mean-square surface roughness is ~5 nm. (n) SEM image of premade checkerboard structures consisting of 1 μm × 1 μm squares. (o) Checkerboard structures covered by ice resist. (p) Patterned 3 × 3 square arrays overlap underneath checkerboard structures completely. (q) An additional exposed area within the red circle reveals the premade square structures under the ice. Dot-dash lines indicate the outline of premade square. All scale bars are 1 μm.

As a lithography technique, an important parameter that needs to be discussed is the speed of iEBL. Like conventional EBL, it is a serial lithography process and therefore inherently slow. We have to recognize that iEBL will take much longer time than conventional EBL to expose the same-sized area, as the dose using water ice is roughly 3 orders of magnitude higher than the typical dose using popular PMMA resist. For iEBL, the production throughput using a beam current of 100 pA is 0.12 μm^2/min. However, much more time will be wasted on loading and unloading steps during conventional EBL. Considering the process time for repetitive development and lift-off steps, we estimate iEBL is less time-consuming in this case. The solution for efficiently improving the throughput of iEBL is to using multiple electron beams simultaneously. Advances in multi-e-beam technology promise to produce high throughput with 600000 parallel e-beams[39].

Generally, alignment process is necessary for overlaying patterns on the previously fabricated layers in 3D nanofabrication. For standard EBL processing, alignment marks should be fabricated

together with the first layer structure and used as the reference to provide a universal coordinate among different layers. Unfortunately, alignment error is usually large (~μm)[40], which seriously affects the fabrication accuracy of 3D nanostructures. In contrast, iEBL allows clear recognition of the shapes and locations of previously fabricated structures covered by ice resist, thus use them as alignment marks. In this way, we are able to reduce the alignment error to sub-100 nm (Figures 2a-2i). Figure 2n-2q gives a better demonstration for the registration ability of iEBL. Figure 2n shows premade checkerboard structures consisting of 1 μm × 1 μm squares. After covered with ice resist (Figure 2o), this sample is exposed by e-beam to produce a 3 × 3 square array encircled by the premade squares (Figure 2p). The outline of our exposed square is perfectly matched with the premade square (Figure 2q). As a fair comparison, the alignment error is typically about 500 nm using PMMA resist in our EBL system.

Due to the particular interaction between electron beam and water ice, it is possible to remove only the top part of ice resist within the exposure area during iEBL, meanwhile, the bottom part survives. This paves the way for iEBL to fabricate another kind of 3D nanostructure by carefully designing the dose distribution in the layout. The basic idea of this fabrication strategy is shown in Figure 3a, where T-shape cross-section appears in the ice resist after a single exposure step. The thickness of resist after exposure is controlled by e-beam dose (Figure 3b), which is similar to the gray-scale lithography method[41]. For a 600-nm-thick ice resist exposed by a 20 keV e-beam, a dose of 0.4 C/cm^2 can be used to remove around 40% ice within the exposure area, and 25% ice will survive if the dose of 0.6 C/cm^2 is employed. The ice gets totally eliminated with dose over 0.7 C/cm^2. Here, the calculated contrast γ is 2.24 at 20 keV (for PMMA, γ = 5-10), indicating water ice is a low contrast resist. Figure 3b also shows the contrast curve at 5 keV and its slope becomes

much sharper. A 3D mushroom-shaped Ag nanostructure is realized after metal deposition and lift-off (Figure 3c), where a top-layer disk with 3-μm diameter is supported on a 2 μm bottom-layer pillar with 170 nm height. In the same way, a bridge-shaped Ag nanostructure with a height of 250 nm, a span of 1.8 μm and a width of 300 nm, is fabricated (Figure 3d). This iEBL fabrication strategy is self-aligned instead of overlay alignment by standard EBL, and much easier than that of using two or more kinds of polymer resists to transfer patterns and protect the substrate. Furthermore, this strategy can be conveniently combined with the stacking layer strategy to achieve complex 3D nanodevices, such as optical resonator[42] and optical modulator[43].

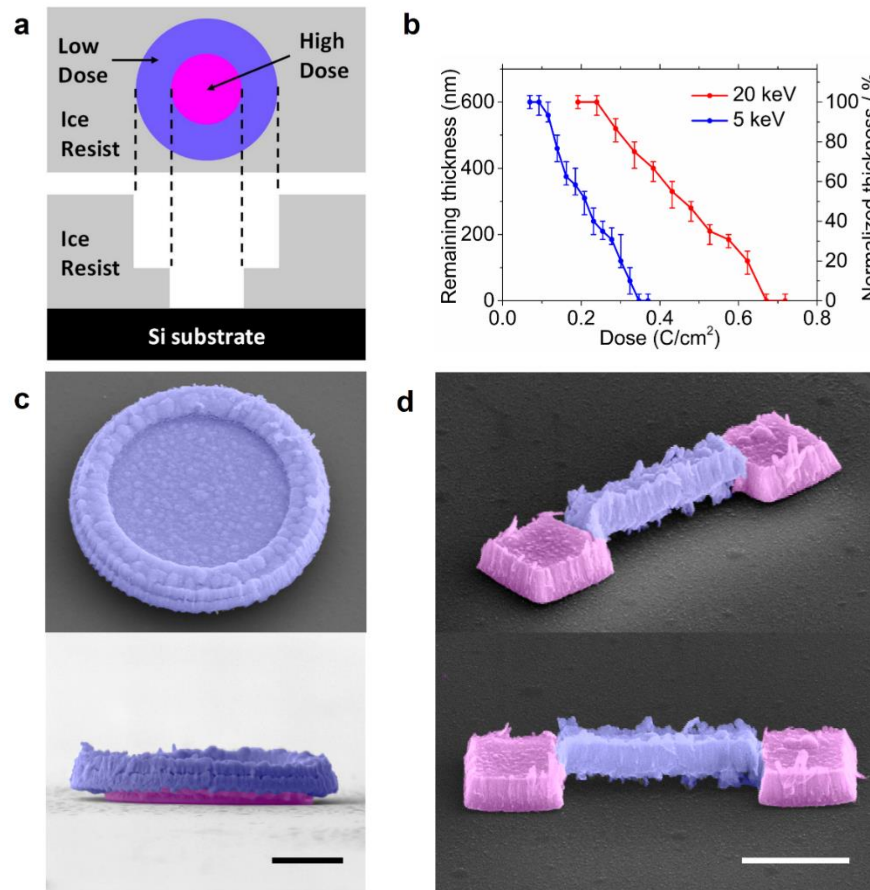

Figure 3. 3D mushroom-shaped and bridge-shaped Ag nanostructures fabricated by iEBL. (a) Typical dose distribution in the designed exposure layout and T-shape cross-section in ice resist after exposure. (b) Contrast curves with error bars in 600-nm-thick ice resist at 5 keV and 20 keV.

(c) False colored SEM images of 3D mushroom-shaped Ag nanostructure. (d) False colored SEM images of bridge-shaped Ag nanostructure. All scale bars are 1 μm.

Finally, we show the potential of iEBL on the fabrication of high-aspect-ratio nanostructures, dense lines, and metallic nanoparticles on a single nanowire. The minimum linewidth of 20 nm has been achieved for ice resists with different thickness. It is clearly observed that 20-nm-wide line patterns penetrate through a 300-nm-thick ice resist layer in Figure 4b (i.e., an aspect ratio of 15). Excluding the influence of the vibration in our system, the minimum linewidth has the potential to be reduced to sub-10 nm[33]. We also expose dense line arrays to demonstrate the high-resolution capability of iEBL. Dense lines with a period of 90 nm are exposed over 5 μm × 5 μm area in 340-nm-thick ice (Figure 4c). The dose is 0.75 μC/cm at 10 keV. Due to low contrast of water ice, the exposed pattern will become deformed when further shrinking the distance between adjacent lines. This ice mask of high aspect ratio could be further processed through integrating a cryogenic etching instrument with our system. In order to explore more possibilities of 3D nanofabrication using iEBL, metallic nanoparticle arrays on a single Ag nanowire with a diameter of 160 nm are demonstrated in Figure 4d. This structure could be hardly obtained by conventional EBL, as the nanowire might move away and be totally lost under PMMA resist during spin-coating. Here, it is very conspicuous that nanoholes after e-beam exposure and metallic particles after metallization are neatly arranged onto the nanowire, which not only evidence the powerful registration ability of iEBL again, but also provide a new way to realize nanowire photonic devices.

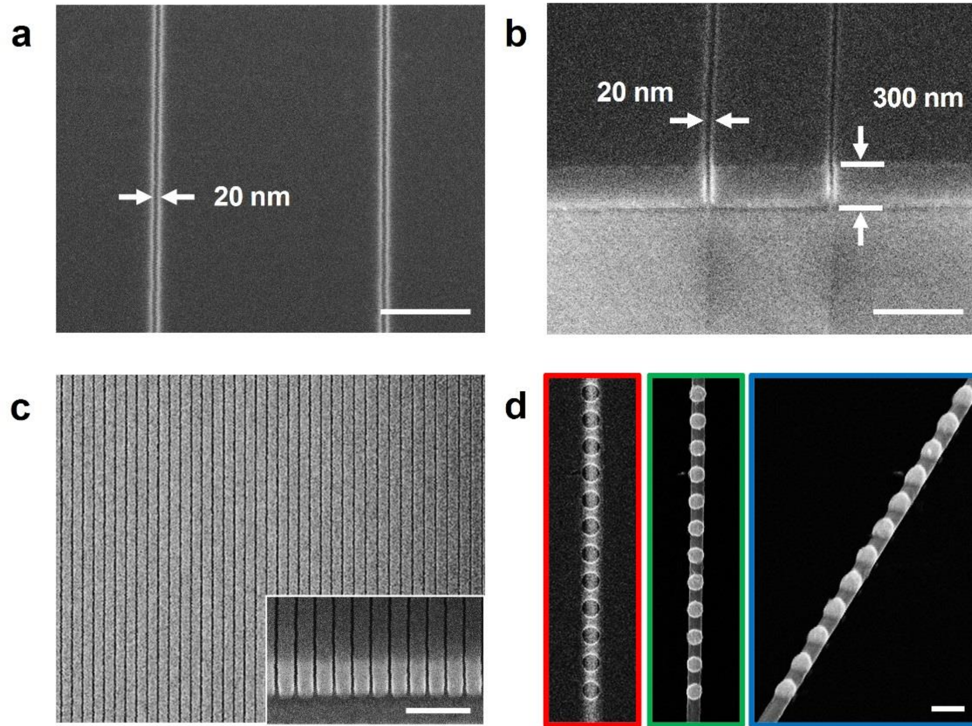

Figure 4. Potential high-aspect-ratio nanostructures, dense lines, and metallic nanoparticles on a single nanowire fabricated by iEBL. (a) Top-view and (b) cross-sectional SEM images (60-degree tilt) of 20-nm-wide line patterns formed in ice resists with thickness of 100 nm and 300 nm, respectively. The e-beam patterning dose is 0.96 μC/cm at 20 keV. (c) Top and tilted views (inset) of dense lines with period of 90 nm exposed in 340-nm-thick ice. The dose is 0.75 μC/cm at 10 keV. (d) Top (green frame) and tilted views (blue frame) of metallic nanoparticle arrays on a single Ag nanowire with diameter of 160 nm. The SEM image with red frame shows the nanowire after e-beam exposure but before metallization. All scale bars are 300 nm.

In summary, we have developed a 3D nanofabrication method using water ice. As a modified technique based on EBL, iEBL can hardly fabricate arbitrary structures, but it works certainly better than conventional EBL in position registration, especially for the structures need overlayer exposure. Here, two types of 3D nanostructures are realized to demonstrate features of this

approach. One is the stepped pyramid nanostructure fabricated by stacking layers. Due to the low sensitivity of water ice, it spends more time on e-beam exposure than using PMMA, meanwhile, this low sensitivity enables *in situ* alignment with previous layers or examination of exposed patterns, which is impossible for both organic ice and conventional EBL resists since SEM imaging will seriously expose them. The other one is mushroom-shaped nanostructure (as well as bridge-shaped nanostructure) realized by dose-modulated exposure. It shows water ice is suitable for grayscale lithography as it has low contrast, but not good for patterning very dense structures. Overall, the iEBL technique needs much fewer processing steps and is almost contamination-free compared to conventional EBL techniques for 3D nanofabrication. It shows great potential in the fabrication of complicated 3D nanodevices for almost all applications, and the only boundary left is our imagination.

ASSOCIATED CONTENT

Supporting Information.

Instrument details, measurement of ice thickness, dimensions of ice patterns and corresponding metal structures, and process details including comparison of standard EBL and iEBL (PDF)

AUTHOR INFORMATION

Corresponding Author

*Email: (D.Z.) dingzhao@zju.edu.cn

*Email: (M.Q.) qiumin@westlake.edu.cn

Author Contributions

Experimental work on ice patterning and characterization was carried by Y.H., as conceived and discussed together with D.Z. and M.Q.; D.Z., Y.H., and D.L. performed modification of SEM in collaboration with A.H.; D.Z., B.M., G.Y. and Q.L. constructed metal deposition chamber. Y.H. and D.Z. drafted the manuscript; all authors contributed to revisions and comments and discussed the results. ‡These authors contributed equally.

Funding Sources

The authors gratefully acknowledge the supports from the National Key Research and Development Program of China (No. 2017YFA0205700), National Natural Science Foundation of China (61425023) and China Postdoctoral Science Foundation (2017M621921).

Notes

The authors declare no competing financial interest.

ACKNOWLEDGMENT

The authors thank Prof. Kehui Wu (Institute of Physics, Chinese Academy of Science) and Prof. Zhihua Gan (Zhejiang University) for helpful comments on vacuum system design and cryogenic solution. We are also grateful to Hanmo Gong, Hao Luo and Pintu Ghosh for their assistance and valuable inputs.

REFERENCES

(1) Zhou, L.; Tan, Y. L.; Wang, J. Y.; Xu, W. C.; Yuan, Y.; Cai, W. S.; Zhu, S. N.; Zhu, J. *Nat. Photonics* **2016,** 10, 393-398.

(2) Lee, J. H.; Koh, C. Y.; Singer, J. P.; Jeon, S. J.; Maldovan, M.; Stein, O.; Thomas, E. L. *Adv. Mater.* **2014,** 26, 532-568.

(3) Khorasaninejad, M.; Chen, W. T.; Devlin, R. C.; Oh, J.; Zhu, A. Y.; Capasso, F. *Science* **2016,** 352, 1190-1194.

(4) Ahn, B. Y.; Duoss, E. B.; Motala, M. J.; Guo, X. Y.; Park, S. I.; Xiong, Y. J.; Yoon, J.; Nuzzo, R. G.; Rogers, J. A.; Lewis, J. A. *Science* **2009,** 323, 1590-1593.

(5) Huang, W.; Yu, X.; Froeter, P.; Xu, R. M.; Ferreira, P.; Li, X. L. *Nano Lett.* **2012,** 12, 6283-6288.

(6) Zhang, F. Y.; Shen, Q. C.; Shi, X. D.; Li, S. P.; Wang, W. L.; Luo, Z.; He, G. F.; Zhang, P.; Tao, P.; Song, C. Y.; Zhang, W.; Zhang, D.; Deng, T.; Shang, W. *Adv. Mater.* **2015,** 27, 1077-1082.

(7) Kong, Y. L.; Gupta, M. K.; Johnson, B. N.; McAlpine, M. C. *Nano Today* **2016,** 11, 330-350.

(8) Gou, M. L.; Qu, X.; Zhu, W.; Xiang, M. L.; Yang, J.; Zhang, K.; Wei, Y. Q.; Chen, S. C. *Nat. Commun.* **2014,** 5, 3774.

(9) Tian, B. Z.; Liu, J.; Dvir, T.; Jin, L. H.; Tsui, J. H.; Qing, Q.; Suo, Z. G.; Langer, R.; Kohane, D. S.; Lieber, C. M. *Nat. Mater.* **2012,** 11, 986-994.

(10) Tan, G. Q.; Wu, F.; Yuan, Y. F.; Chen, R. J.; Zhao, T.; Yao, Y.; Qian, J.; Liu, J. R.; Ye, Y. S.; Shahbazian-Yassar, R.; Lu, J.; Amine, K. *Nat. Commun.* **2016,** 7, 11774.

(11) Zhang, H. G.; Yu, X. D.; Braun, P. V. *Nat. Nanotechnol.* **2011,** 6, 277-281.

(12) Sun, K.; Wei, T. S.; Ahn, B. Y.; Seo, J. Y.; Dillon, S. J.; Lewis, J. A. *Adv. Mater.* **2013,** 25, 4539-4543.

(13) Sirringhaus, H.; Kawase, T.; Friend, R. H.; Shimoda, T.; Inbasekaran, M.; Wu, W.; Woo, E. P. *Science* **2000,** 290, 2123-6.

(14) Gratson, G. M.; Xu, M.; Lewis, J. A. *Nature* **2004,** 428, 386.

(15) Zhang, A. P.; Qu, X.; Soman, P.; Hribar, K. C.; Lee, J. W.; Chen, S.; He, S. *Adv. Mater.* **2012,** 24, 4266-70.

(16) Farahani, R. D.; Dube, M.; Therriault, D. *Adv. Mater.* **2016,** 28, 5794-5821.

(17) Park, J. U.; Hardy, M.; Kang, S. J.; Barton, K.; Adair, K.; Mukhopadhyay, D. K.; Lee, C. Y.; Strano, M. S.; Alleyne, A. G.; Georgiadis, J. G.; Ferreira, P. M.; Rogers, J. A. *Nat. Mater.* **2007,** 6, 782-9.

(18) Sun, H. B.; Matsuo, S.; Misawa, H. *Appl. Phys. Lett.* **1999,** 74, 786-788.

(19) Kawata, S.; Sun, H. B.; Tanaka, T.; Takada, K. *Nature* **2001,** 412, 697-8.

(20) Galliker, P.; Schneider, J.; Eghlidi, H.; Kress, S.; Sandoghdar, V.; Poulikakos, D. *Nat. Commun.* **2012,** 3, 890.

(21) Onses, M. S.; Sutanto, E.; Ferreira, P. M.; Alleyne, A. G.; Rogers, J. A. *Small* **2015,** 11, 4237-66.

(22) Li, L.; Gattass, R. R.; Gershgoren, E.; Hwang, H.; Fourkas, J. T. *Science* **2009,** 324, 910-3.

(23) Mao, M.; He, J. K.; Li, X.; Zhang, B.; Lei, Q.; Liu, Y. X.; Li, D. C. *Micromachines* **2017,** 8, 113.

(24) Fowlkes, J. D.; Winkler, R.; Lewis, B. B.; Stanford, M. G.; Plank, H.; Rack, P. D. *ACS Nano* **2016,** 10, 6163-6172.

(25) Pires, D.; Hedrick, J. L.; De Silva, A.; Frommer, J.; Gotsmann, B.; Wolf, H.; Despont, M.; Duerig, U.; Knoll, A. W. *Science* **2010,** 328, 732-5.

(26) Steenackers, M.; Jordan, R.; Kuller, A.; Grunze, M. *Adv. Mater.* **2009,** 21, 2921-+.

(27) Liu, X. Q.; Li, Y.; Zheng, Z. J. *Nanoscale* **2010,** 2, 2614-2618.

(28) Chen, C. J.; Xie, Z.; Wei, X. L.; Zheng, Z. J. *Small* **2015,** 11, 6013-6017.

(29) Chou, S. Y.; Krauss, P. R.; Renstrom, P. J. *Appl. Phys. Lett.* **1995,** 67, 3114-3116.

(30) Zaumseil, J.; Meitl, M. A.; Hsu, J. W. P.; Acharya, B. R.; Baldwin, K. W.; Loo, Y. L.; Rogers, J. A. *Nano Lett.* **2003,** 3, 1223-1227.

(31) Yang, S. M.; Jang, S. G.; Choi, D. G.; Kim, S.; Yu, H. K. *Small* **2006,** 2, 458-475.

(32) Park, M.; Harrison, C.; Chaikin, P. M.; Register, R. A.; Adamson, D. H. *Science* **1997,** 276, 1401-1404.

(33) King, G. M.; Schurmann, G.; Branton, D.; Golovchenko, J. A. *Nano Lett.* **2005,** 5, 1157-1160.

(34) Han, A.; Vlassarev, D.; Wang, J.; Golovchenko, J. A.; Branton, D. *Nano Lett.* **2010,** 10, 5056-9.

(35) Han, A.; Kuan, A.; Golovchenko, J.; Branton, D. *Nano Lett.* **2012,** 12, 1018-21.

(36) Tiddi, W.; Elsukova, A.; Le, H. T.; Liu, P.; Beleggia, M.; Han, A. *Nano Lett.* **2017,** 17, 7886-7891.

(37) Tiddi, W.; Elsukova, A.; Beleggia, M.; Han, A. P. *Microelectron. Eng.* **2018,** 192, 38-43.

(38) Han, A.; Chervinsky, J.; Branton, D.; Golovchenko, J. A. *Rev. Sci. Instrum.* **2011,** 82, 065110.

(39) Hagen, C. W. *Appl. Phys. A: Mater. Sci. Process.* **2014,** 117, 1599-1605.

(40) Yoon, G.; Kim, I.; So, S.; Mun, J.; Kim, M.; Rho, J. *Sci. Rep.* **2017,** 7, 6668.

(41) Waits, C. M.; Morgan, B.; Kastantin, M.; Ghodssi, R. *Sens. Actuators, A* **2005,** 119, 245-253.

(42) Peng, B.; Ozdemir, S. K.; Lei, F. C.; Monifi, F.; Gianfreda, M.; Long, G. L.; Fan, S. H.; Nori, F.; Bender, C. M.; Yang, L. *Nat. Phys.* **2014,** 10, 394-398.

(43) Haffner, C.; Chelladurai, D.; Fedoryshyn, Y.; Josten, A.; Baeuerle, B.; Heni, W.; Watanabe, T.; Cui, T.; Cheng, B. J.; Saha, S.; Elder, D. L.; Dalton, L. R.; Boltasseva, A.; Shalaev, V. M.; Kinsey, N.; Leuthold, J. *Nature* **2018,** 556, 483.

TOC Figure

76.5 x 34.5 mm (300 x 300 DPI)